Peer-Reviewed Technical Communication

Online System Identification of an Autonomous Underwater Vehicle Via In-Field Experiments

You Hong Eng, *Member, IEEE*, Kwong Meng Teo, Mandar Chitre, *Senior Member, IEEE*, and Kien Ming Ng

***Abstract*—The dynamic characteristic of an autonomous underwater vehicle (AUV) is affected when it is reconfigured with different payloads. It is desirable to have an updated model, such that the control and guidance law can be redesigned to obtain better performance. Hence, we develop a method to enable online identification of AUV dynamics via in-field experiments, where the AUV is commanded to execute a compact set of maneuvers under doublet excitation. The identification process has two stages. In the training stage, state variable filter and recursive least square (SVF-RLS) estimator is used to estimate the unknown parameters. In the validation stage, the prediction capability of the model is checked using a fresh data set. The parameters converged within 12 s in the experiments using five different thrusts. Validation results show that the identified models are able to explain 78% to 92% of the output variation. Next, we compare the SVF-RLS estimator with the conventional offline identification method. The comparison shows that the SVF-RLS estimator is better in terms of prediction accuracy, computational cost and training time. The usefulness of the identified models is highlighted in two applications. We use it to estimate the turning radius of the AUV at different speeds, and to design a gain-scheduled controller.**

***Index Terms*—Autonomous underwater vehicles (AUV), system identification.**

I. Introduction

In the last decade, we have seen autonomous underwater vehicles (AUVs) leaving the research laboratory for commercial real world applications [1]. Some commercially available AUVs in the marketplace are *Remus* [2], *Gavia* [3] and *Iver2* [4]. To meet the diverse requirements of the end users, they are modular in design and support reconfiguration with different payloads. Such reconfiguration, however, often affect the dynamic characteristic of the AUV. As the dynamic model underlies the design of its navigation, guidance and control systems, any deviation from its nominal model would potentially degrade its performance [5] or in the worst case, cause critical safety issues.

Manuscript received May 26, 2014; revised October 22, 2014; accepted February 09, 2015. Date of publication March 04, 2015; date of current version January 11, 2016.

Associate Editor: K. von Ellenrieder.

Y. H. Eng and M. Chitre are with the Acoustic Research Laboratory, Tropical Marine Science Institute, National University of Singapore, 119222 Singapore (e-mail: tmseyh@nus.edu.sg).

K. M. Teo and K. M. Ng are with the Department of Industrial and Systems Engineering, National University of Singapore, Singapore.

Digital Object Identifier 10.1109/JOE.2015.2403576

For a modular AUV, one would like to have an updated dynamic model after each change in payload configuration or vehicle geometry. One effective method to obtain the dynamic model is via field experiments of the actual AUV. Before running an actual mission, the AUV is programmed to perform a compact set of maneuvers. Vehicle response is then measured using on-board sensors. Based on the vehicle response under known excitation, the unknown parameters of the dynamic model are determined. Such an approach, which allows AUV dynamics to be identified more rapidly, is called on-board system identification by Caccia *et al.* [6], or in-field identification by Mišković *et al.* [7].

Most of the on-board system identification methods reported for unmanned underwater vehicles (UUVs) are offline operated and mostly applied to open-frame vehicles. Caccia *et al.* [6] identified a lump parameter model of ROMEO, an open-frame UUV, using least square method and took into consideration the propeller-hull and propeller-propeller interaction effect. Ridao *et al.* [8] compared two identification methods using URIS UUV: one is based on the minimization of the acceleration prediction error, and the other, on the minimization of the velocity one-step prediction error. An online adaptive identification technique had been proposed by Smallwood and Whitcomb [9] for application in their JHUROV remotely operated underwater vehicle (ROV). For applications on streamlined AUVs, work had been done by Rentschler *et al.* [10] where parameter estimation was performed offline using an optimization technique. Tiano *et al.* [11] proposed to use an observer Kalman filter identification method to identify yaw dynamics of the Hammerhead AUV. Both simulation and experimental results were presented, but the online implementation of their algorithm was not discussed in detail.

The principal aim of this paper is to propose an economical and feasible method to obtain a reasonably accurate dynamic model of the AUV via in-field experiments. Compared with previous works, the proposed method allows identification to be done more rapidly. The identification results are available immediately after each experimental run, and hence can be utilized in the design of the controller and guidance law without human intervention. This could result in considerable improvements in system performances and substantial savings in ship-time. The identified parameters could also be used to monitor the health status of the AUV, allowing early fault detection before running an actual mission [12].

The key features of our method are described as follows:

- We circumvent the nonlinearity of the AUV dynamics by approximating the nonlinear model via parameter scheduling technique. The AUV speed is used to characterize the scheduling, where a local linear time-invariant (LTI) model is identified at each speed. Then, several LTI models are identified at speeds spanning the whole operating range, resulting in a linear-parameter-varying (LPV) model [13], which is valid within the identified range.
- We construct the LTI model in continuous-time domain, instead of a discrete-time domain, as used in [11]. This preserves the physical meaning of the identified parameters, which turns out to be extremely useful in analysis and application. From the analysis perspective, it allows easy verification of the result by comparing it against our physical understanding of the AUV. From the application point of view, we could identify the model for two extreme speeds and obtain models for intermediate speeds via interpolation. The dynamic behavior of the AUV can be approximated beyond the identified range, assuming that the model can be extrapolated.
- While the state variable filter (SVF) and recursive least-square (RLS) estimator (SVF-RLS) approach to continuous-time model identification is well known [14], the application to AUVs and the experimental evaluation reported here are new. The proposed method is simpler to implement and requires fewer design parameters to be selected when compare with the existing methods using adaptive identifier [9] and nonlinear observer [15].
- We validate the method through extensive field experiments on our in-house built STARFISH AUV [16]. Similar to many other available AUVs, the STARFISH AUV is torpedo in shape, has a single thruster and four control fins at the rear. The identification method requires limited instrumentation; in fact, it only requires a compass module, which is a standard equipment among AUVs. Hence, we believe the proposed method is widely applicable.
- While only yaw dynamics is discussed here, the proposed method could be extended to pitch dynamics as well, as reported in [17]. Discussion of pitch dynamics is omitted here for simplicity and clarity.
- The proposed identification process has two main stages. Unknown model parameters are estimated in the training stage, and then validated in the validation stage. Prediction capability of the identified model is checked using a fresh validation data set instead of the old training data set. Such procedures, known as *cross-validation*, make sense without any probabilistic arguments and without any assumptions about the true system [18].

The paper is organized as follows. In Section II, we introduce the simplified model that describes the yaw dynamics of the AUV. The identification method is discussed in Section III. The details of experimental procedures and results are discussed in Section IV. In Section V, we compare the SVF-RLS estimator against conventional offline identification method. Two applications of the identification models are shown in Section VI: prediction of the AUV's turning radius at different speeds and design of a gain-scheduled controller for heading control. Lastly, some concluding remarks are presented in Section VII.

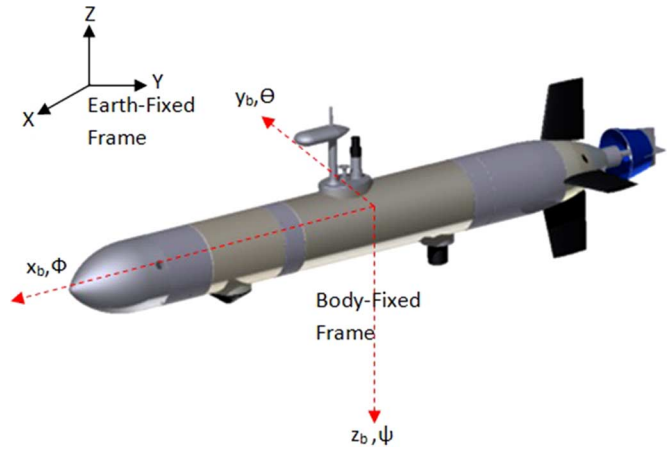

Fig. 1. Reference frame of STARFISH AUV.

II. Modeling of Yaw Dynamics

Generally, the motion of an AUV can be described using six degrees of freedom differential equations of motion [19]. These equations are developed using two coordinate frames shown in Fig. 1. Six positions and attitudes components $[x, y, z, \phi, \theta, \psi]$ (surge, sway, heave, roll, pitch, yaw) are defined in the earth-fixed frame, while the corresponding velocity and angular rate components $[u, v, w, p, q, r]$ are defined in the body-fixed frame.

When designing a controller for the AUV, we follow the conventional control philosophy that divides the AUV into three subsystems [20]. They are the:

1) steering subsystem, which controls the heading by using the rudder;
2) diving subsystem, which controls the depth and pitch by using the elevator;
3) speed subsystem, which controls the vehicle speed by varying the propeller speed.

The divide-and-conquer methodology works well in practice for streamlined AUVs when the coupling between subsystems is weak.

From [20], the yaw dynamics has the following state-space representation using state variables $v(t), r(t), \psi(t)$:

$$\begin{bmatrix} \dot{v} \\ \dot{r} \\ \dot{\psi} \end{bmatrix} = \begin{bmatrix} a_{11} & a_{12} & 0 \\ a_{21} & a_{22} & 0 \\ 0 & 1 & 0 \end{bmatrix} \begin{bmatrix} v \\ r \\ \psi \end{bmatrix} + \begin{bmatrix} b_1 \\ b_2 \\ 0 \end{bmatrix} \delta_{\mathrm{r}} \tag{1}$$

where a_{ij} and b_i are hydrodynamic coefficients, and δ_{r} is rudder deflection.

Specifically, yaw dynamics is described by the following equation:

$$\dot{r} = a_{21} v + a_{22} r + b_2 \delta_{\mathrm{r}}. \tag{2}$$

From experimental results, the sway velocity v is small during operation. In addition, the coefficient a_{21} is also small for torpedo-shaped AUV since it is almost symmetrical in the y-z plane (bow and stern). Thus, the yaw dynamics can be further simplified to

$$\dot{\psi} = r \tag{3}$$

$$\dot{r} = a_{22} r + b_2 \delta_{\mathrm{r}}. \tag{4}$$

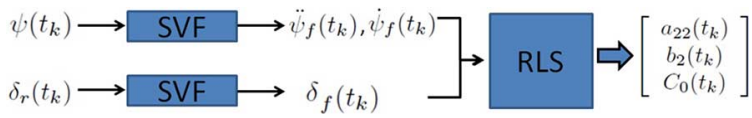

Fig. 2. Dataflow in SVF-RLS estimator.

We extend the model by adding an extra term, called steady state rudder deflection δ_0 as shown below

$$\dot{\psi} = r \tag{5}$$
$$\dot{r} = a_{22} r + b_2(\delta_\mathrm{r} + \delta_0). \tag{6}$$

In particular, δ_0 is the rudder deflection when yaw angle is constant. Under normal condition, δ_0 should be equal to zero. However, it can be nonzero under the following circumstances:

1) When there is misalignment between the rudder zero position and vehicle vertical plane. This misalignment can be due to calibration error or accidental impact on the rudder.
2) When there is strong cross-current. In this case, sway velocity v is not small, such that δ_0 will capture the ignored term a_{21} in (1).
3) When there is asymmetry in x-z plane (port and starboard) of the AUV. The asymmetry causes higher drag on one side of the AUV, resulting in a yaw moment that needs to be compensated by rudder deflection.

Rewriting (6), we have linear-in-parameters model with three unknowns

$$\dot{r} = \begin{bmatrix} r & \delta_\mathrm{r} & 1 \end{bmatrix} \begin{bmatrix} a_{22} \\ b_2 \\ C_0 \end{bmatrix} \tag{7}$$

where $C_0 = b_2\delta_0$.

The three unknown parameters are: rotational drag coefficient a_{22}, rudder control authority b_2, and steady state rudder deflection δ_0. For easy reference, hereafter, we denote the unknown parameters as the following parameter vector:

$$\Theta = [a_{22}, b_2, C_0]^\top. \tag{8}$$

Applying a Laplace Transform and a change of variable to (6), we have

$$\frac{\boldsymbol{\Psi}(s)}{\boldsymbol{\Delta}'(s)} = \frac{b_2}{s^2 - a_{22}s}, \quad \boldsymbol{\Psi}(s) = \mathcal{L}\{\psi(t)\}$$
$$\boldsymbol{\Delta}'(s) = \mathcal{L}\{\delta_\mathrm{r}(t) - \delta_0\}. \tag{9}$$

We circumvent the nonlinearity of the AUV dynamics by approximating the nonlinear model via parameter scheduling technique. The AUV speed is used to characterize the scheduling: a local linear time-invariant (LTI) model (7) is identified at a particular speed, then several LTI models are identified across speeds of interest, resulting in a LPV model. In other words, for each particular speed u, we have a set of three parameters

$$\Theta_u = [a_{22}, b_2, C_0]^\top. \tag{10}$$

III. Identification Method

Fig. 2 gives an overview on how $\Theta(t_k)$ is generated at every sampling instant, t_k by feeding rudder deflection $\delta_\mathrm{r}(t_k)$ and yaw measurement $\psi(t_k)$ into the SVF-RLS estimator. State variable filter (SVF) is used to produce filtered signals, $\ddot{\psi}_\mathrm{f}(t_k), \dot{\psi}_\mathrm{f}(t_k)$ and $\delta_\mathrm{f}(t_k)$. The filtered signals are later used in recursive least square (RLS) to produce $\Theta(t_k)$.

A. Problem Formulation

Equation (7) can be written in the following form:

$$\frac{d^2\psi}{dt^2} - a_{22}\frac{d\psi}{dt} = b_2\delta_\mathrm{r}(t) + C_0. \tag{11}$$

The equation describes a single-input, single-output, linear, time-invariant, continuous-time system having noise-free input $\delta_\mathrm{r}(t)$ and output $\psi(t)$. The system is proper. It is assumed that the input and output signals are sampled at time instants $\{t_k\}_{k=1}^N$. The sampled input and output signals at instant k are denoted by $\delta_\mathrm{r}(t_k)$ and $\psi(t_k)$ respectively.

The identification problem consists of using input/output discrete data $\{\delta_\mathrm{r}(t_k); \psi(t_k)\}, k = 1 \ldots . N$, to determine the values of parameters a_{22}, b_2, and C_0 while satisfying certain goodness-of-fit constraints between predicted data and measurement. N is the total number of samples available. Then $\Theta^\top$ could be solved as

$$\underset{\Theta^\top=[a_{22},b_2,C_0]}{\arg\min} \; J(\Theta) = \sqrt{\frac{1}{N}\sum_{k=1}^{k=N}[\ddot{\psi}(t_k) - \Theta^\top\Phi(t_k)]^2}$$
$$\text{subject to } a_{22}, b_2, C_0 \in \Re \tag{12}$$

where

$$\Phi(t_k) = [\,\dot{\psi}(t_k) \quad \delta_\mathrm{r}(t_k) \quad 1\,]^\top. \tag{13}$$

For the cost function $J(\Theta)$ defined in (12), we have two time derivatives: $\ddot{\psi}(t_k)$ and $\dot{\psi}(t_k)$, which are not available from any instrument. We employ state variable filter to reconstruct the two time derivatives from ψ. So, $\Theta^\top$ could be solved as

$$\underset{\Theta^\top=[a_{22},b_2,C_0]}{\arg\min} \; J(\Theta) = \sqrt{\frac{1}{N}\sum_{k=1}^{k=N}[\ddot{\psi}_\mathrm{f}(t_k) - \Theta^\top\Phi_\mathrm{f}(t_k)]^2}$$
$$\text{subject to } a_{22}, b_2, C_0 \in \Re \tag{14}$$

where

$$\Phi_\mathrm{f}(t_k) = [\,\dot{\psi}_\mathrm{f}(t_k) \quad \delta_\mathrm{f}(t_k) \quad 1\,]^\top. \tag{15}$$

B. State Variable Filter

Reconstructing the time derivative from sampled data is an important step in direct continuous-time model identification. It is well known that numerical computation of the derivative

via finite difference method is very sensitive to measurement noise. The problem is overcome by traditional SVF approach by passing both input/output signals through an all-pole filter $F(s)$ of minimum order n. It is preferable to choose $F(s)$ such that it has n similar poles [21]

$$F(s) = \frac{\lambda^n}{(s+\lambda)^n}. \tag{16}$$

The numerator is chosen to be λ^n instead of 1 such that the filter has a unity dc gain. λ has to be chosen to match the bandwidth of the system dynamics. In particular, λ has to be chosen large enough, such that the filtered signal contains useful information of the dynamics, and small enough to filter out the measurement noise. According to [22], state variable filter serves as a prefilter, and selection of λ allows one to emphasize certain frequency regions where model mismatch should be small.

Let

$$\boldsymbol{\psi}_\mathbf{f}(t) = [\,\ddot{\psi}_\mathrm{f}(t) \quad \dot{\psi}_\mathrm{f}(t) \quad \psi_\mathrm{f}(t)\,]^\top. \tag{17}$$

$$\tag{18}$$

Denote the Laplace transforms of $\psi(t)$ and $\delta_\mathrm{r}(t)$ as

$$\boldsymbol{\Psi}(s) = \mathcal{L}\{\psi(t)\} \tag{19}$$

$$\boldsymbol{\Delta}(s) = \mathcal{L}\{\delta_\mathrm{r}(t)\}. \tag{20}$$

Then

$$\begin{aligned}\boldsymbol{\Psi}_\mathbf{f}(s) &= \mathcal{L}\{\boldsymbol{\psi}_\mathbf{f}(t)\} \\ &= \frac{\lambda^2}{(s+\lambda)^2}[\,s^2 \quad s \quad 1\,]^\top \boldsymbol{\Psi}(s). \end{aligned}\tag{21}$$

$$\begin{aligned}\boldsymbol{\Delta}_\mathbf{f}(s) &= \mathcal{L}\{\delta_\mathrm{f}(t)\} \\ &= \frac{\lambda^2}{(s+\lambda)^2}\boldsymbol{\Delta}(s). \end{aligned}\tag{22}$$

Note that the above filters are causally implementable. Here, we give a specific example on numerical implementation of the filter. The implementation is adopted from [21]. To obtain the time-derivative of order two, we need the following filter:

$$\mathbf{F(s)} = \left[\,\frac{\lambda^2 s^2}{(s+\lambda)^2} \quad \frac{\lambda^2 s}{(s+\lambda)^2} \quad \frac{\lambda^2}{(s+\lambda)^2}\,\right]^\top. \tag{23}$$

Let us denote the input signal to the filter as $w(t)$. The following state-space equations written in controllable canonical form can be used to obtain the filter output:

$$\mathbf{y}(t) = \left[\,w_\mathrm{f}^{(2)} \quad w_\mathrm{f}^{(1)} \quad w_\mathrm{f}^{(0)}\,\right]^\top. \tag{24}$$

$$\mathbf{x}(t) = \left[\,w_\mathrm{f}^{(1)} \quad w_\mathrm{f}^{(0)}\,\right]^\top. \tag{25}$$

$w_\mathrm{f}^{(2)}, w_\mathrm{f}^{(1)}$ and $w_\mathrm{f}^{(0)}$ are the second, first, and zeroth derivative of the filter input $w(t)$ respectively

$$\dot{\mathbf{x}}(t) = \mathbf{A}\mathbf{x}(t) + \mathbf{B}w(t) \tag{26}$$

$$\mathbf{y}(t) = \mathbf{C}\mathbf{x}(t) + \mathbf{D}w(t) \tag{27}$$

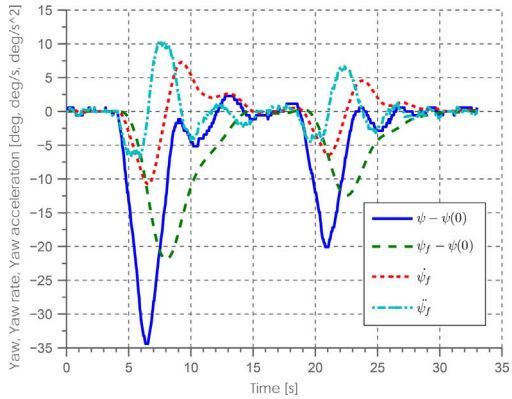

Fig. 3. Input and Output of the SVF filter for $\lambda = 1$.

with

$$\mathbf{A} = \begin{bmatrix} -2\lambda & -\lambda^2 \\ 1 & 0 \end{bmatrix}, \quad \mathbf{B} = \begin{bmatrix} 1 \\ 0 \end{bmatrix}$$

$$\mathbf{C} = \lambda^2 \begin{bmatrix} -2\lambda & -\lambda^2 \\ 1 & 0 \\ 0 & 1 \end{bmatrix}, \quad \mathbf{D} = \lambda^2 \begin{bmatrix} 1 \\ 0 \\ 0 \end{bmatrix}. \tag{28}$$

Under zero order hold (ZOH) assumption and with sampling interval, $h_k = t_{k+1} - t_k$, the above state-space can be discretized into

$$\dot{\mathbf{x}}(t_{k+1}) = \mathbf{A_d}\mathbf{x}(t_t) + \mathbf{B_d}w(t_k) \tag{29}$$

$$\mathbf{y}(t_k) = \mathbf{C_d}\mathbf{x}(t_k) + \mathbf{D_d}w(t_k) \tag{30}$$

with

$$\begin{aligned}&\mathbf{A_d} = e^{\mathbf{A}h_k}, \mathbf{B_d} = [e^{\mathbf{A}h_k} - \mathbf{I}]\mathbf{A}^{-1}\mathbf{B} \\ &\mathbf{C_d} = \mathbf{C}, \mathbf{D_d} = \mathbf{D}. \end{aligned}\tag{31}$$

Fig. 3 illustrates the experimentally measured yaw ψ and its corresponding filtered output for $\lambda = 1$.

C. Recursive Least Square (RLS)

Parameters in optimization problem (14) can be identified experimentally using standard least square method. Let N denote the total number of measurements available, and we define

$$Q = [\,\ddot{\psi}_\mathrm{f}(t_1) \quad \ddot{\psi}_\mathrm{f}(t_2) \cdots \quad \ddot{\psi}_\mathrm{f}(t_N)\,]^\top \tag{32}$$

and

$$\boldsymbol{\Phi} = \begin{bmatrix} \dot{\psi}_\mathrm{f}(t_1) & \delta_\mathrm{f}(t_1) & 1 \\ \dot{\psi}_\mathrm{f}(t_2) & \delta_\mathrm{f}(t_2) & 1 \\ \vdots & \vdots & \vdots \\ \dot{\psi}_\mathrm{f}(t_N) & \delta_\mathrm{f}(t_N) & 1 \end{bmatrix}. \tag{33}$$

Thus if $\boldsymbol{\Phi}$ is full rank, then the least square solution is given by the standard Moore–Penrose pseudoinverse

$$\hat{\Theta} = (\boldsymbol{\Phi}^\top \boldsymbol{\Phi})^{-1} \boldsymbol{\Phi}^\top Q. \tag{34}$$

The idea behind RLS is to compute the parameters update $\hat{\Theta}(t)$ at each time instant t when measurements become available, by adding a correction term to the previous estimate $\hat{\Theta}(t-1)$. This saves a lot of computational effort as compare with the use of (34) with the entire measurement. It reduces the computational complexity from $O(N^3)$ to $O(N^2)$. For time-invariant system, the system parameters Θ are constant.

Fig. 4. STARFISH AUV equipped with DVL and LEDIF payload at the Pandan Reservoir, Singapore.

A typical RLS algorithm consists of the following recursive equations [23]:

$$\begin{aligned}\hat{\Theta}(t_k) &= \hat{\Theta}(t_{k-1}) + K(t_k)\epsilon(t_k)\\ \epsilon(t_k) &= \ddot{\psi}_{\mathrm{f}}(t_k) - \hat{\Theta}^{\top}(t_{k-1})\Phi_{\mathrm{f}}(t_k)\\ K(t_k) &= \frac{P(t_{k-1})\Phi_{\mathrm{f}}(t_k)}{1+\Phi_{\mathrm{f}}^{\top}(t_k)P(t_{k-1})\Phi_{\mathrm{f}}(t_k)}\\ P(t_k) &= \left[1 - K^{\top}(t_k)\Phi_{\mathrm{f}}(t_k)\right]P(t_{k-1}).\end{aligned}$$

The algorithm requires an initial guess of $\Theta(t)$ and the error covariance matrix P. The initial guess of $\Theta(t)$ is the zero vector and P is $100\mathbf{I}_3$, where $\mathbf{I}_3$ is the identity matrix of dimension 3.

D. Validation Method

Model validation is one of the important steps in any identification process. One needs to be assured that the identified model is an accurate representation of the system. One commonly seen method is to perform identification (training) on all the repeated experiments and then compare the identified parameters for consistency. In our opinion, this is not a test on the validity of the model, but rather a test on the repeatability of the experiment. To test the predictability of the model, one needs to test the model on fresh or untrained data set. As pointed out by ([18], pg. 500),

> It is not so surprising that a model will be able to reproduce the training data. The real test is whether it will be capable of also describing fresh data sets from the process.

The experiments are designed to collect two different data sets: *training data* are the data that would be used to estimate unknown parameters; *validation data* are fresh data that have not been used for parameter estimation. Using the validation data, simulated yaw responses, ψ_{sim} are generated by feeding the real rudder inputs into the identified model. Then it is possible to know how well the identified model can predict the measured yaw responses ψ_{real} by comparing ψ_{sim} to ψ_{real}. The goodness-of-fit between the two is measured using the coefficient of determination, R^2, defined as

$$R^2 = 1 - \frac{J_{\mathrm{k}}}{\mathrm{Var}(\psi_{\mathrm{real}})} \tag{35}$$

where

$$J_{\mathrm{k}} = \frac{1}{n}\sum_{i=1}^{n}(\psi_{\mathrm{sim}} - \psi_{\mathrm{real}})^2 \tag{36}$$

and

$$\mathrm{Var}(\psi_{\mathrm{real}}) = \frac{1}{n}\sum_{i=1}^{n}(\psi_{\mathrm{real}} - \bar{\psi}_{\mathrm{real}})^2. \tag{37}$$

$\bar{\psi}_{\mathrm{real}}$ is the mean value of ψ_{real}. Basically, R^2 indicates what fraction of the variance of the experiment data is explained by the simulated response. An R^2 value of 1 means a perfect fit and the model has captured 100% of the output variation.

TABLE I
SENSORS

Sensor	Measurement	Model	Manufacturer
Compass	Roll, Pitch & Yaw	HMR3500	Honeywell
Pressure	Depth	PDCR 1830	General Electric
DVL	Speed	Explorer	Teledyne

IV. Field Experiments

A. Research Platform

The STARFISH, an AUV built in-house, serves as an ideal platform to test the proposed method. The STARFISH AUV is highly modular in design, which allows easy reconfiguration of the vehicle's payloads according to mission requirement. In Fig. 4, the STARFISH AUV is equipped with LED induced fluorescence (LEDIF) payload for in-situ real-time optical sensing of the water chemistry, and Doppler Velocity Log (DVL) payload for enhanced navigation capability. The mass of the vehicle is 65 kg and it is 2.3 m long with a diameter of 0.2 m. Currently, there are also the sidescan payload and thin-line array (TLA) payload in our lineup. Depending on the payload configuration, changes in vehicle geometry and its dynamics would be expected. So, the proposed method serves to fulfill the needs of identification of vehicle dynamics after each change in payload configuration.

The base STARFISH is equipped with a number of sensors. As far as this work is concerned, a compass module for attitude measurement, a pressure sensor for depth measurement, and a doppler velocity log (DVL) for speed measurement are used. Their details are tabulated in Table I. DVL is an expensive sensor and may not be available for certain low-cost AUVs. It is to be emphasized that speed measurement is not necessary in our proposed method. The AUV speed u and thrust τ have a static relationship at steady state and it is known that $\tau \propto u^2$. So, the dynamic model can be scheduled by thrust instead of speed. On the other hand, the angular position of the rudder is not measured. It is assumed that the angular position is the same as the commanded angle sent to the servomotor. This assumption holds as the response time of the servomotor is many times faster than the yaw dynamics.

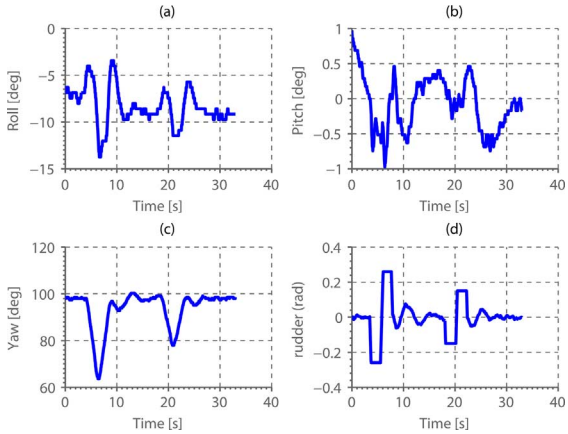

Fig. 5. Experimental run for identification of yaw dynamics at 100% thrust. Plot of roll, pitch, yaw and rudder.

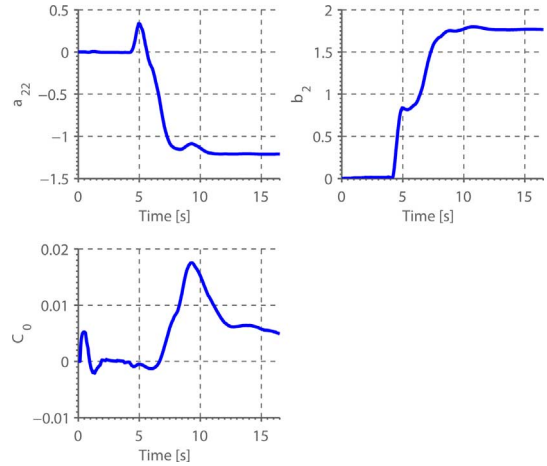

Fig. 6. Online parameter estimation of yaw dynamics at 100% thrust. Unknown parameters a_{22}, b_2, and C_0 have initial values of zero.

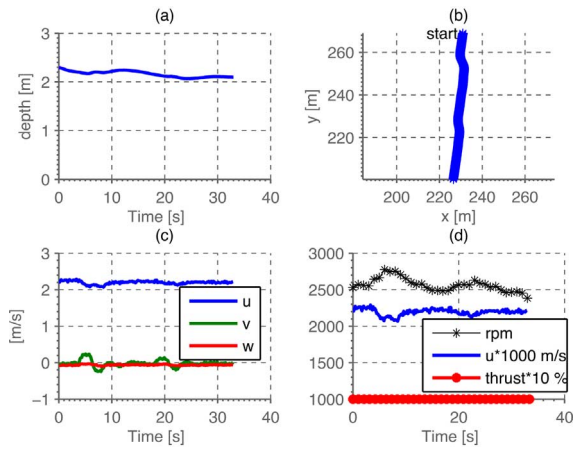

Fig. 7. Experimental run for identification of yaw dynamics at 100% thrust. Plot of depth, x-y position, velocity, and thrust settings.

B. Experimental Setup & Procedure

After changing the payload, the newly configured AUV needs to be trimmed for buoyancy, static pitch and roll angle. This is normally done by resting the AUV in a water tank. Then, the AUV is trimmed to have 7 N positive buoyancy[1] and static pitch and roll angle around zero by adding or changing the weight distribution of the vehicle. The purpose is to configure the AUV to a default state, so that an initial conservative controller is capable of controlling it to the operating condition where identification could be carried out. Such an initial controller is not difficult to be found heuristically, as pointed out by Rentschler *et al.* [10].

In the following, we will discuss different stages executed by the AUV during a typical identification run. In stage 1, the AUV is commanded to perform a straight run at a depth of 2 m with a constant thrust. It is allowed to settle down into the steady state (maintaining a constant heading, velocity and depth) within 40 s.

In stage 2 (training stage), the SVF-RLS estimator is turned on to start the estimation of the parameters. After 2 s, an excitation signal (doublet) of amplitude 0.26 rad for a period of 4 s is injected into the rudder deflection [see Fig. 5(d)]. The deflection generates a moment around the yaw axis and excites the yaw dynamics dramatically [see Fig. 5(c)]. After the excitation, the yaw controller is reengaged to return the AUV to the desired heading. The SVF-RLS estimator is stopped after 10.5 s from the end of excitation. Stage 2 takes 16.5 s in total, with 330 data points processed at the rate of 20 Hz. The identification is only enabled during the resultant zig-zag maneuvering to fulfill the persistent excitation condition and to have a better signal-to-noise ratio (SNR). The unknown parameters, namely a_{22}, b_2, C_0 are estimated on-the-fly at every sampling instant (see Fig. 6). The unknown parameters would converge and the last values are taken to be the final results. The results are then stored in the database for that particular thrust, and $\Theta(t)$ and $P(t)$ in RLS are reinitialized.

In stage 3 (validation stage), the second excitation signal (doublet) of amplitude[2] 0.15 rad for a period of 4 s is injected into the rudder deflection [see Fig. 5(d)]. It is important to point out that there is no parameter estimation in this stage. The whole purpose is to collect a fresh data set for cross-validation. We generate the simulated yaw response, ψ_{sim} by feeding the real rudder inputs into the model defined by the parameters estimated in stage 2. Stage 3 takes 16.5 s in total, with 330 data points recorded. Measured yaw responses, ψ_{real}, are recorded to calculate the coefficient of determination, R^2, at the end of stage 3.

During the identification process, the depth [see Fig. 7(a)] and pitch [see Fig. 5(b)] are kept approximately constant, and the roll is small [see Fig. 5(a)] to minimize the coupling effect. The AUV is moving in a straight path as shown in Fig. 7(b) except when the excitation signal is injected. The identification procedures are repeated for five different thrust values: 60%, 70%, 80%, 90%, and 100% before the AUV is commanded to the preset home location.

C. Experimental Results

The results presented in this section were collected at Pandan Reservoir[3], Singapore. The base STARFISH AUV is equipped with a DVL payload and a sidescan payload. Identification was done under five different thrust settings: ranging from 60% to 100%.

[1]It is the buoyancy required to keep the AUV communication tower above water surface.

[2]Different amplitudes are used to excite the dynamics. We would like to test whether the dynamics remain the same under different excitation.

[3]Pandan Reservoir located in the western region of Singapore.

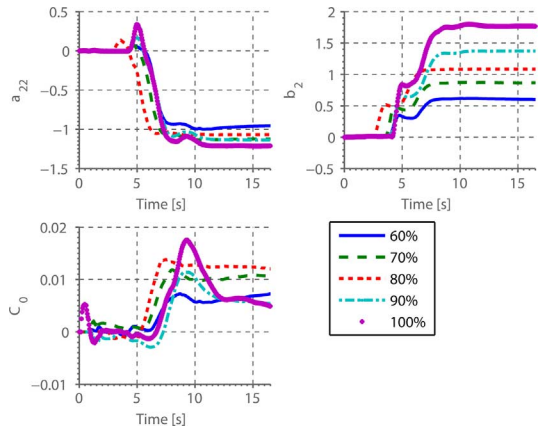

Fig. 8. Online parameter estimation of yaw dynamics for different thrusts.

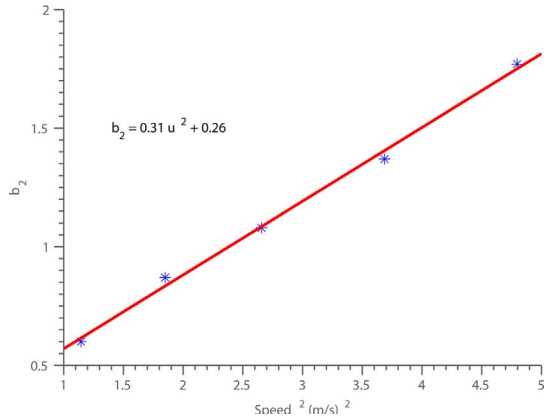

Fig. 9. Rudder control authority b_2 as a function of square of speed.

TABLE II
PARAMETERS IDENTIFIED THROUGH THE SVF-RLS ESTIMATOR AT FIVE DIFFERENT THRUST SETTINGS WITH AUV CONFIGURATION: (BASE + DVL + SIDESCAN)

Thrust (%)	Speed (m/s)	a_{22} (1/s)	b_2 (1/s^2)	C_0 (rad/s^2)	δ_0 (rad)	R^2
60	1.07	-0.95	0.60	0.0072	0.012	0.780
70	1.36	-1.12	0.87	0.0107	0.012	0.916
80	1.63	-1.07	1.08	0.0120	0.011	0.890
90	1.92	-1.14	1.37	0.0054	0.004	0.900
100	2.19	-1.21	1.77	0.0049	0.003	0.852

Fig. 8 shows online parameter estimation of the three unknown parameters for five different thrust settings. For every thrust setting, all three parameters converged after about 12 s. The results are summarized in Table II. The negative value of rotational drag coefficient a_{22} indicates that the yaw dynamics is inherently stable (poles are in the left-half plane). The a_{22} values have small variation around its mean value of 1.1 when thrust setting is varied.

The rudder control authority b_2 increases with speed due to higher dynamic pressure at the control surfaces. Theoretically, the gain b_2 should vary linearly with the square of speed, u^2. This is verified in Fig. 9 which plots b_2 against u^2. The positive value of b_2 indicates that a positive rudder input creates a positive moment in yaw and vice versa. The steady state rudder deflection δ_0 reduces with increase in speed. This is due to the increase of control authority which requires smaller fin deflection to overcome the same yaw disturbance. The value of δ_0 is almost zero. This indicates that there was no significant misalignment of fins. This corresponds with the fact that the rudder position was calibrated before the trial. In addition, there was no significant cross-current at the reservoir and the AUV is symmetrical in port and starboard.

From the last column of Table II, it is observed that R^2 ranges from 0.780 to 0.916, which indicates that the models are able to explain 78% to 92% of the yaw output variation. The variation of R^2 values is expected as the experiments were conducted in unstructured real world environment, subjected to unknown disturbance and measurement noise. Nevertheless, the overall prediction capabilities are satisfactory as one could see

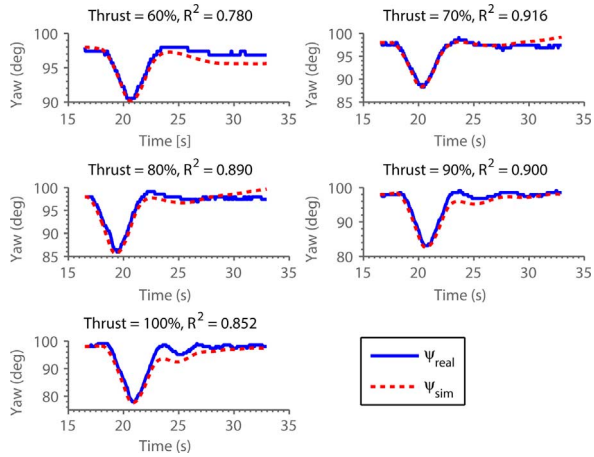

Fig. 10. Validation plots for experiments on five different thrust settings. Identified models are able to explain 78% to 92% of the yaw output variation.

in Fig. 10, which overlays both ψ_{real} and ψ_{sim} for thrust 60% to 100% and their corresponding R^2 values. The simulated response ψ_{sim} is able to describe the measured response very well for all thrust settings. From the results, we are convinced that the identified models have captured the dominant dynamic characteristic of the process. Based on all the conducted experiments, the smallest R^2 obtained so far is 0.61, in which the corresponding identified parameters are still reasonably accurate. So, as a rule of thumb, one could repeat the identification for that particular speed when the R^2 obtained from validation step is less than 0.60.

V. COMPARISON WITH CONVENTIONAL OFFLINE METHOD

From Section IV-C, we have validated the accuracy of the model identified by the SVF-RLS estimator based on R^2 values. However, it is interesting to study how the SVF-RLS estimator performs when compare with other identification methods. Here, we compare our online identification method against the conventional offline identification method that requires optimization via simulation.

The simulation takes in rudder input $\delta_{\text{r}}(t_k)$ along with the AUV initial states (yaw angle and yaw rate) and simulates the vehicle's response ψ_{sim} using (11), which is defined by an initial

TABLE III
PARAMETERS IDENTIFIED THROUGH THE CONVENTIONAL OFFLINE METHOD AT FIVE DIFFERENT THRUST SETTINGS WITH AUV CONFIGURATION: (BASE + DVL + SIDESCAN)

Thrust (%)	a_{22} (1/s)	b_2 (1/s^2)	C_0 (rad/s^2)	δ_0 (rad)	R^2	Number Iteration
60	-0.98	0.61	0.0078	0.013	0.888	103
70	-1.20	0.88	0.0125	0.014	0.741	81
80	-1.19	1.12	0.0149	0.013	0.756	67
90	-1.32	1.48	0.0072	0.005	0.957	137
100	-1.42	1.85	0.0073	0.004	0.941	125

guess of Θ. At the end of every simulation, the following cost function is calculated:

$$J_{\text{offline}}(\Theta) = \sqrt{\frac{1}{N}\sum_{k=1}^{k=N}[\psi_{\text{real}}(t_k) - \psi_{\text{sim}}(t_k)]^2}. \quad (38)$$

The optimization process searches iteratively for Θ that minimizes the cost function by repeating the simulation with different Θ. The optimization was conducted in Matlab/Simulink™ using the Parameters Estimation Toolbox in this study. The optimization method is Simplex search [24]. The initial guess of parameters Θ is the zero vector. There are two stopping criteria. The first criterion is to set the parameter tolerance to 0.01 as it is the accuracy of the parameters reported in this paper. The second criterion is to set the function tolerance to 0.0001 to prevent the searching algorithm from stopping prematurely.

The algorithm does not require the time derivative of the yaw. However, it is important to note that simulation can only be run after the entire data set is collected. Hence, identification via simulation can only be executed offline. If the solution space is convex, the numerical optimization will produce an optimal Θ that minimizes the cost function for that particular set of training data. But, this optimality is generally not true for validation data, which are not used in the optimization.

Table III reports the Θ obtained through the offline identification method. From Tables II and III, the parameters are close to each other when comparing the coefficients. However, this is only a qualitative comparison. For quantitative comparison, we should compare the R^2 values produced by both methods. The R^2 for both methods are tabulated in the last column of Tables II and III, respectively. The offline identification method achieved on average an R^2 value of 0.857 whereas the online identification method achieved on average an R^2 value of 0.868. Hence, both methods achieve similar performance in terms of the accuracy of the prediction.

The difference in Θ estimation can be explained by the difference in cost functions used. The cost function for the offline method (38) is defined as the mean square error between the simulated yaw response and measured yaw response, whereas the cost function for the online method (14) is defined as the mean square error between the predicted yaw acceleration and measured yaw acceleration[4]. Fig. 11 overlays ψ_{sim} for both online and offline methods for training data and validation data respectively. The offline method achieved better overall fit but the online method had better fit when the AUV was turning. By

[4]The measured yaw acceleration is generated from measured yaw via state variable filter.

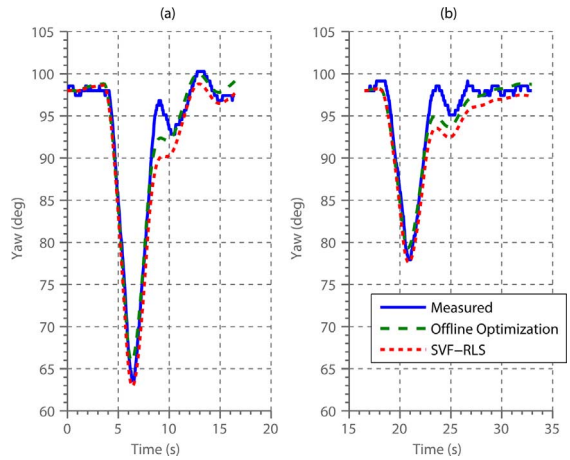

Fig. 11. Fitting of identified and measured yaw angle at 100% thrust for both online and offline methods. (a) Training. (b) Validation.

the definition of the cost function, the online method puts more weight on the portion of data where the AUV experienced larger yaw acceleration. Since the interest is in the dynamic part of the yaw response, the online method produces better estimates in this aspect.

In terms of computational cost, the online method is much cheaper than the offline method. The offline method requires simulation of the whole data set at each search iteration. In each simulation run, the simulated yaw response ψ_{sim} is computed using the fourth-order Runge–Kutta ordinary differential equation (ODE) integrator. Table III shows that it took around 100 iterations on average for the parameters to converge.

Online identification allows one to monitor the convergence of the parameters on-the-fly. Some stopping criteria can be used to stop the parameter training once it is believed that the parameters have attained the desired accuracy. One such criterion is by monitoring the Euclidean norm of the change of the parameter estimate in every time instance to be less than a specific value, such as 0.001. In mathematical notations, the criterion is expressed as

$$\|\Theta(t_k) - \Theta(t_{k-1})\|_2 < 0.001. \quad (39)$$

Fig. 12 shows that the criterion was first met from 12 s onward for all five thrust settings. In practice, the criterion should be met consecutively for a certain number of times before the training is stopped. This is to prevent the premature termination of the training. The ability to know parameter convergence online allows training to be stopped early and hence saves valuable experiment time. As shown in Fig. 12, training could be stopped as early as 12 s instead of 16.5 s.

From the above discussions, we conclude that the online identification method compares favorably against the conventional offline method in terms of accuracy, computational cost, and capability to stop training early.

VI. APPLICATIONS

The ultimate validation is to test whether the problem that motivated the modeling exercise can be solved using the obtained model ([18], pg. 509).

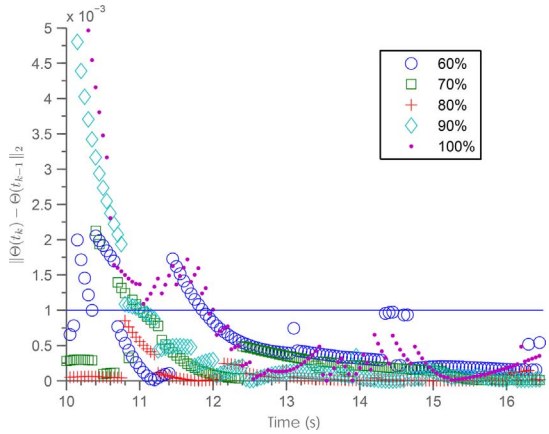

Fig. 12. Norm of the step change of the parameters Θ. All step changes are smaller than 0.001 after 12 s.

In this section, we discuss two applications of the identified model.

A. Turning Radius of AUV at Different Speeds

The yaw identification results could be used to estimate the turning radius of the AUV at different speeds. An understanding of the turning radius is especially important during maneuvering of the AUV for obstacle avoidance. It is also useful during path planning so that the achievable turning angle is taken into consideration (See Dubins curves in [25]).

We assume that the AUV has completed the yaw identification such that the information present in Table II is available. For each speed, we require information on travel speed V, control authority b_2, and linear damping a_{22}. The rudder has a maximum deflection $\delta_{\max}$ of 0.26 rad to avoid stalling.

Fig. 13(a) illustrates an AUV making a U-turn with radius R. The perimeter of the half circle is πR. Let T_π denote the time taken to make a 180 deg turn. Then, we have

$$\pi R = V T_\pi. \tag{40}$$

Fig. 13(b) shows a trapezoidal profile for yaw angular velocity. To make a U-turn, the AUV will start turning from zero yaw angular velocity to critical yaw angular velocity, $\dot{\psi}_{\max}$. The acceleration process takes t_1 s. Then, it maintains the turning rate at $\dot{\psi}_{\max}$ for t_2 s before decelerating to zero. The deceleration process takes another t_1 s, and so

$$T_\pi = t_1 + t_2 + t_1. \tag{41}$$

The area under the curve is the total heading change of π rad. So

$$\frac{1}{2}\dot{\psi}_{\max}(t_2 + t_1 + t_2 + t_1) = \pi \tag{42}$$

which gives

$$\dot{\psi}_{\max}(t_2 + t_1) = \pi. \tag{43}$$

From (9), we know that the transfer function of yaw angular velocity to rudder is a first-order system

$$\frac{s\Psi(s)}{\Delta'(s)} = \frac{b_2}{s - a_{22}}. \tag{44}$$

Under the step input of rudder at magnitude $(\delta_{\max} - \delta_0)$, the step response is

$$C(S) = \frac{b_2}{s - a_{22}} \cdot \frac{\delta_{\max} - \delta_0}{s}. \tag{45}$$

Taking the inverse transform, the step response is given by

$$c(t) = \frac{b_2(\delta_{\max} - \delta_0)}{-a_{22}}(1 - e^{a_{22}t}). \tag{46}$$

By letting $t \to \infty$ in (46), $\dot{\psi}_{\max}$ is given by

$$\dot{\psi}_{\max} = \frac{b_2(\delta_{\max} - \delta_0)}{-a_{22}}. \tag{47}$$

The time t_1 is approximated by the time taken to reach 100% of the final value ([26], pg. 180)

$$t_1 = \frac{4}{-a_{22}}. \tag{48}$$

Substituting (43), (47) and (48) into (41), we have

$$T_\pi = -\left(\frac{\pi a_{22}}{b_2(\delta_{\max} - \delta_0)} + \frac{4}{a_{22}}\right), \tag{49}$$

and

$$R = -V\left(\frac{a_{22}}{b_2(\delta_{\max} - \delta_0)} + \frac{4}{a_{22}\pi}\right). \tag{50}$$

Table II suggests that the drag coefficient a_{22} stays constant at -1.1. From Fig. 9, we have the following relationship between speed V and b_2 (sign of b_2 is dropped as the absolute value of b_2 is used)

$$b_2 = 0.31V^2 + 0.26. \tag{51}$$

With $\delta_{\max} = 0.26$ rad and $\delta_0 = 0$, we have

$$R = -V\left(\frac{-1.1}{(0.31V^2 + 0.26)(0.26)} + \frac{4}{(-1.1)\pi}\right). \tag{52}$$

Similarly, we have $\dot{\psi}_{\max}$ and T_π as follows:

$$\dot{\psi}_{\max} = \frac{0.26(0.31V^2 + 0.26)}{1.1} \tag{53}$$

$$T_\pi = \frac{1.1\pi}{0.26(0.31V^2 + 0.26)} + \frac{4}{1.1}. \tag{54}$$

Fig. 14 predicts how $R, \Psi_{\max}$ and T_π change with speed. It is important to note that yaw identification was only performed for a speed range from 1 to 2.2 m/s but the plot shows the results for speeds from 0.5 to 5 m/s. The result is only valid if (51) and the assumption $a_{22} = -1.1$ holds also for speeds ranging from 0.5 to 5 m/s.

The critical yaw angular velocity $\dot{\psi}_{\max}$ increases with speed. From (47), $\dot{\psi}_{\max}$ is linearly proportional to b_2, which in turn is linearly proportional to the square of speed. As expected, the time taken to complete a U-turn, T_π, reduces with speed as the AUV turns at a faster rate.

The results show that the AUV should travel at lower speeds to achieve a smaller turning radius. For example, at speed 0.25 m/s, the turning radius is 4 m. The trade-off is that it takes about 48 s to complete a U-turn. For the higher speed region, the minimum achievable turning radius is 5.9 m at a speed of 4.2

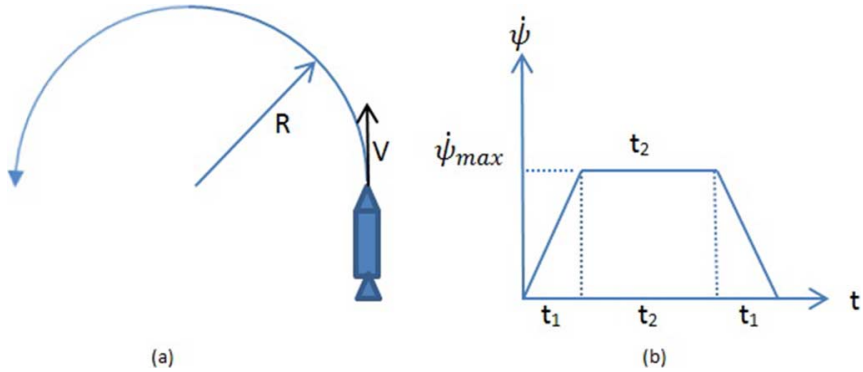

Fig. 13. (a) Turning radius R of an AUV traveling at speed, V and (b) trapezoidal profile for yaw angular velocity.

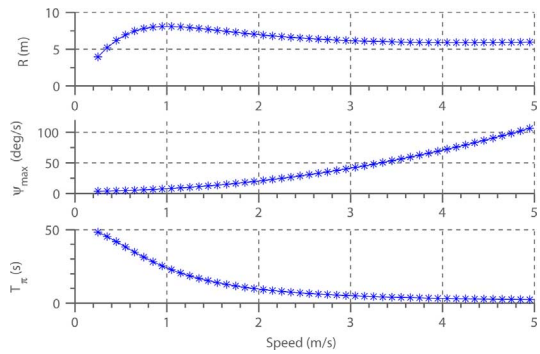

Fig. 14. Turning radius of AUV at different speeds.

m/s. [5]The turning radius increases with speed after that. There is a minimum value for T_π despite an increase in speed. As $R \propto VT_\pi$, when V increases faster than the decrease in T_π, the turning radius will increase with speed.

A field experiment was carried out to compare the measured turning radius against the predicted turning radius. A base AUV with a doppler velocity log (DVL) payload was used in this experiment. The AUV was commanded to a constant depth of 2 m. It was commanded to thrust at 70% with an average speed of 1.4 m/s. Yaw identification was executed to identify parameters a_{22}, b_2 and C_0. Then the AUV was commanded to make a U-turn before returning to the surface. The turning radius of the AUV was found by fitting a circle on the x-y position plot as illustrated in Fig. 15(a). Table IV shows the identified parameters and the predicted $\dot{\psi}_{\max}, T_\pi$ and R. It is interesting to note that δ_0 is not equal to zero. In this case, the effective maximum rudder deflection $\delta_{\max}$ is $0.26 - 0.04 = 0.22$ rad. The predicted turning radius is 9.2 m, which is close to the measured turning radius of 9.9 m. The prediction is accurate as a result of good modeling of the yaw rate[6] as can be seen in Fig. 15(b).

In this subsection, we have illustrated how the turning radius can be calculated from the identified parameters. By postulating that the model can be extrapolated, we study the turning radius of the AUV beyond the speed region where it was identified. The results indicate that the turning radius has a local minimum

[5]The STARFISH AUV design top speed is only about 2.5 m/s, so this speed is not achievable in practice.

[6]Measured yaw rate is derived from yaw measurement using Savitzky-Golay filter.

TABLE IV
TURNING RADIUS FOR AUV: A CASE STUDY WITH AUV CONFIGURATION: (BASE + DVL)

a_{22}	b_2	δ_0	$\dot{\psi}_{\max}$ (deg/s)	T_π (s)	R (m)
-1.62	1.25	0.04	9.90	20.65	9.20

at the high speed region where we cannot reduce the turning radius by increasing the speed further. On the other hand, traveling slowly is the way to reduce the turning radius, but this is at the expense of longer turning time. Lastly, via a field experiment, we show that the turning radius can be predicted accurately based on the identified parameters.

B. Gain-Scheduled Controller Design

The main purpose of system identification is to reconfigure the controller according to the system dynamics. We next present some results on the steering control of the STARFISH AUV at different speeds. We would like to demonstrate the ease of controller synthesis after the parameters are obtained and highlight the performance improvements after reconfiguration.

Fig. 16 shows the block diagram of the steering control system. We close the loop using a simple proportional (P) controller with a feedforward term. There are two main problems in steering control at different speeds. The yaw dynamics changes with speed. One possible solution is to use robust control design methodology, which results in selecting a constant gain, $K_{\rm p}$ that minimizes the norm of the closed-loop transfer function under parametric uncertainty. However, a constant gain robust controller can be very conservative as compare with a gain-scheduled controller that can adapt itself to the change in system dynamics. Another problem in steering control is the steady state error caused by nonzero rudder offset. We handle the problem by feed-forwarding δ_0 to neutralize the offset.

From the block diagram, the closed-loop transfer function from the desired yaw $\psi_{\rm d}$ to yaw output ψ is

$$\frac{\psi_{\rm d}(s)}{\psi(s)} = \frac{K_{\rm p} b_2}{s^2 - a_{22}s + K_{\rm p} b_2}. \tag{55}$$

The closed-loop poles are

$$p_{1,2} = \frac{a_{22}}{2} \pm \frac{\sqrt{a_{22}^2 - 4K_{\rm p} b_2}}{2}. \tag{56}$$

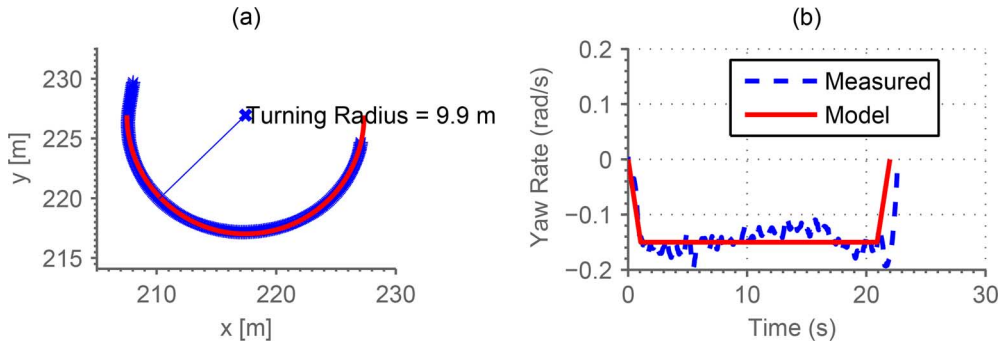

Fig. 15. (a) Turning radius of AUV during the case study (b) Measured yaw rate and modeled yaw rate during the U-turn.

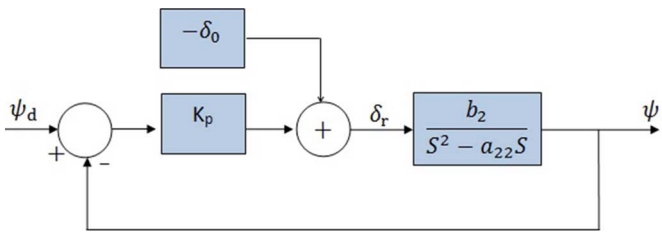

Fig. 16. Block diagram for heading control.

TABLE V
PARAMETERS IDENTIFIED THROUGH THE SVF-RLS ESTIMATOR AT DIFFERENT THRUST SETTINGS WITH AUV CONFIGURATION: (BASE + DVL + TLA)

Thrust (%)	Speed (m/s)	a_{22} (1/s)	b_2 (1/s^2)	C_0 (rad/s^2)	δ_0 (rad)	R^2	K_p
60	1.05	-1.28	0.65	0.0129	0.016	0.614	1.26
70	1.32	-1.51	1.04	0.0169	0.020	0.977	1.09
80	1.60	-1.70	1.41	0.0274	0.019	0.973	1.02
80	1.60	-1.54	1.30	0.0273	0.021	0.848	0.91
90	1.87	-1.69	1.85	0.0163	0.009	0.911	0.77
100	2.13	-1.48	2.02	0.0312	0.016	0.911	0.54

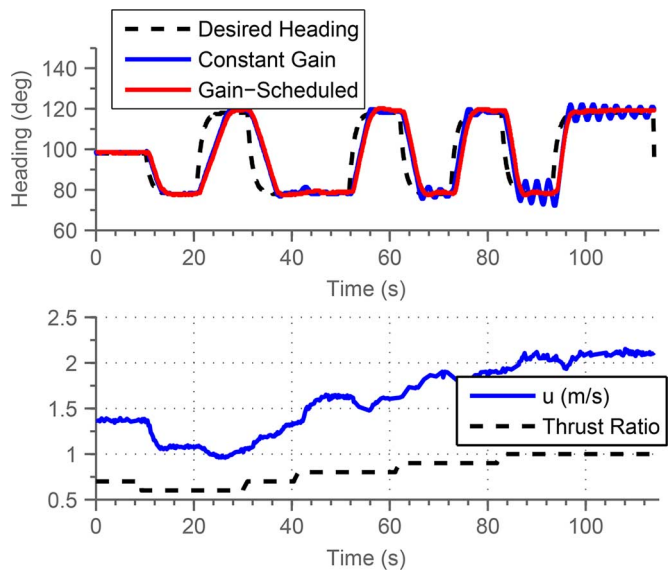

Fig. 17. Experimental results for heading control under constant gain controller and gain-scheduled controller.

We select gain K_p such that the closed-loop poles lie in the line of constant damping ratio ζ in the s-plane. For a second order system, the overshoot percentage is only a function of damping ratio. So, we choose ζ to be 0.7071, which is equivalent to approximately 5% overshoot. In the *s-plane*, constant damping ratio line of 0.7071 corresponds to the $y = -x$ line. Hence, we require

$$-a_{22}^2 = a_{22}^2 - 4K_p b_2 \Longrightarrow K_p = \frac{a_{22}^2}{2b_2}. \tag{57}$$

As shown in Table V, a_{22} and b_2, which are functions of speed, were identified before the design of the gain-scheduled controller. At different speeds, the gain K_p will be adjusted accordingly as tabulated in the last column of Table V.

We repeated the identification experiment twice for 80% thrust to check the repeatability of the experiment. We observed a small different in the estimation of the parameters; the first experiment estimated $\hat{\Theta}_1 = [-1.70, 1.41, 0.0274]$ and the second experiment estimated $\hat{\Theta}_2 = [-1.54, 1.30, 0.0273]$. We should set the gain, K_p to 1.02 if based on the $\hat{\Theta}_1$, and set the K_p to 0.91 if based on the $\hat{\Theta}_2$. Both experiments also give very close prediction on the turning radius (50), they are 9.20 and 9.25 m for $\hat{\Theta}_1$ and $\hat{\Theta}_2$, respectively. Although there are some small variations in the identified parameters, which is expected due to measurement noise and disturbances, both $\hat{\Theta}$ give consistent suggestion on the controller gain K_p and the turning radius.

The experimental results obtained using the gain-scheduled controller with feedforward are shown in Fig. 17 with comparison to a constant gain controller. The AUV was first commanded to maintain a constant depth and heading. Then the AUV was commanded to turn ± 20 deg from the current heading while the thrust was increased from 60% to 100%. The constant gain controller performed satisfactorily at the lower speed as the constant gain was determined based on manual tuning when the AUV was operating at 60% thrust. In the higher speed region (90% and 100% thrust), the heading response became oscillatory. In contrast, the gain-scheduled controller consistently performed well over the entire speed envelop.

One interesting question: how gain K_p should be set when the operating thrust fall between the identified thrust, such as the value of K_p when the thrust is 65%? K_p can be set via interpolation. Let us explain. First, we plot the K_p values at different thrusts in Fig. 18, which indicates that the gain K_p is decreasing linearly with the increasing of thrust. If the identification was only performed at 60% and 100% thrust, we would only know

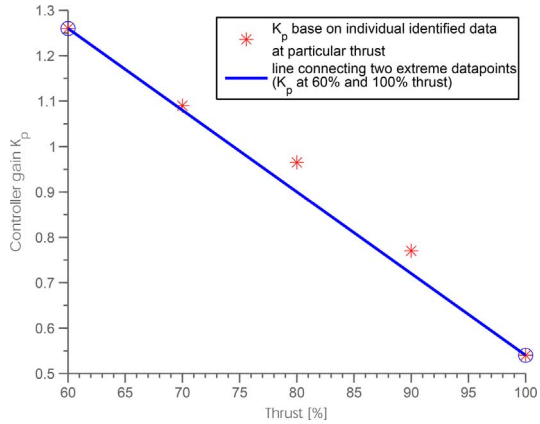

Fig. 18. Controller gain K_p at different thrusts.

the K_p at the two extreme points. Then, we can infer the K_p for intermediate thrust by interpolation, which is indicated by the straight line connecting the two extreme points. The plot shows that the K_p obtained from the interpolation matches the K_p obtained via the individual identified results at 70%, 80%, and 90% thrust, respectively. This has an important practical implication: our proposed controller can be designed by performing identification at the two extreme thrusts and then the intermediate gain can be inferred via interpolation.

VII. Conclusion

We have developed a method to enable rapid identification of AUV dynamics via in-field experiments. The method could be employed to obtain an updated dynamic model economically whenever there is a change in payload configuration or vehicle geometry. The newly configured AUV is commanded to perform a compact set of maneuvers where doublet excitation is used to excite the yaw dynamics. The identification process has two main stages. In the training stage, the rudder inputs and yaw measurements are processed online by the SVF-RLS estimator to produce estimation of the unknown model parameters. In the validation stage, the prediction capability of the identified model is checked using fresh validation data sets. For experiments on five different thrust settings, the parameters show fast convergence within 12 s. Validation results show that the identified models are able to explain 78% to 92% of the yaw output variation and hence we are convinced that the identified models have captured the dominant characteristics of the dynamics. The identification results indicate that the rotational drag coefficient a_{22} has small variation around its mean when the speed varies. The rudder control authority b_2 varies linearly with the square of speed u^2 which matches well with our physical understanding. These observations are important because they allow us to predict the yaw model beyond those identified through experiments, via interpolation or extrapolation.

We compare the SVF-RLS estimator against a conventional offline identification method that requires numerical optimization. The comparison shows that the SVF-RLS estimator outperforms the offline method in terms of prediction accuracy, computational cost and shorter training time by detecting parameter convergence online. The usefulness of the identified parameters is highlighted in two applications. We illustrate how the yaw identification results can be used to estimate the turning radius of the AUV at different speeds. The accuracy of the estimation is validated in a field experiment. The understanding of yaw dynamics at different speeds allows easy implementation of a gain-scheduled controller. The experimental results indicate that the gain-scheduled controller achieved better system performance compare with a constant gain controller.

References

[1] D. R. Blidberg, "The development of autonomous underwater vehicles (AUVs); a brief summary," in *Proc. IEEE ICRA*, 2001, vol. 6500.
[2] K. Maritime, 2014, Remus [Online]. Available: http://www.km.kongsberg.com/auv
[3] T. T. Incorporated, 2014, Gavia [Online]. Available: http://www.teledynegavia.com/
[4] I. OceanServer Technology 2014, Iver2 [Online]. Available: http://iver-auv.com/
[5] L. Shirtley, P. Formby, M. Bell, and S. Anstee, "Modification of a Nose Cone for a REMUS 100 Autonomous Underwater Vehicle to Improve Low-Speed Stability," 2009.
[6] M. Caccia, G. Indiveri, and G. Veruggio, "Modeling and identification of open-frame variable configuration unmanned underwater vehicles," *IEEE J. Ocean. Eng.*, vol. 25, no. 2, pp. 227–240, 2000.
[7] N. Mišković, Z. Vukić, M. Bibuli, G. Bruzzone, and M. Caccia, "Fast in-field identification of unmanned marine vehicles," *J. Field Robot.*, vol. 28, no. 1, pp. 101–120, 2011.
[8] P. Ridao, A. Tiano, A. El-Fakdi, M. Carreras, and A. Zirilli, "On the identification of non-linear models of unmanned underwater vehicles," *Contr. Eng. Pract.*, vol. 12, no. 12, pp. 1483–1499, 2004.
[9] D. Smallwood and L. Whitcomb, "Adaptive identification of dynamically positioned underwater robotic vehicles," *IEEE Trans. Control Syst. Technol.*, vol. 11, no. 4, pp. 505–515, Jul. 2003.
[10] M. Rentschler, F. Hover, and C. Chryssostomidis, "System identification of open-loop maneuvers leads to improved AUV flight performance," *IEEE J. Ocean. Eng.*, vol. 31, no. 1, pp. 200–208, Apr. 2006.
[11] A. Tiano, R. Sutton, A. Lozowicki, and W. Naeem, "Observer kalman filter identification of an autonomous underwater vehicle," *Contr. Eng. Practice*, vol. 15, no. 6, pp. 727–739, 2007.
[12] A. Healey, "Towards an automatic health monitor for autonomous underwater vehicles using parameter identification," in *Proc. Amer. Contr. Conf.*, 1993, pp. 585–589, IEEE.
[13] J. Mohammadpour and C. Scherer, *Control of Linear Parameter Varying Systems With Applications*. Berlin, Germany: Springer-Verlag, 2012.
[14] H. Garnier, M. Gilson, T. Bastogne, and M. Mensler, "The contsid toolbox: A software support for data-based continuous-time modelling," *Identification Continuous-Time Models From Sampled Data*, pp. 249–290, 2008.
[15] J. Kim, K. Kim, H. Choi, W. Seong, and K. Lee, "Depth and heading control for autonomous underwater vehicle using estimated hydrodynamic coefficients," in *Proc. MTS/IEEE OCEANS*, 2001, vol. 1, pp. 429–435, IEEE.
[16] T.-B. Koay, Y.-T. Tan, Y.-H. Eng, R. Gao, M. Chitre, J.-L. Chew, N. Chandhavarkar, R. Khan, T. Taher, and J. Koh, "Starfish—A small team of autonomous robotic fish," *Indian J. Geomarine* ., vol. 40, no. 2, pp. 157–167, Apr. 2011.
[17] Y. H. Eng, K. M. Teo, and M. Chitre, "Online system identification of the dynamics of an autonomous underwater vehicle," in *Proc. IEEE Inte. Underwater Technol. Symp. (UT)*, 2013, pp. 1–10.
[18] L. Ljung, *System Identification*. New York, NY, USA: Wiley, 1999.
[19] T. Fossen, *Guidance and Control of Ocean Vehicles*. New York, NY, USA: Wiley, 1994.
[20] B. Jalving, "The NDRE-AUV flight control system," *IEEE J. Ocean. Eng.*, vol. 19, no. 4, pp. 497–501, Oct. 1994.
[21] K. Mahata and H. Garnier, "Direct identification of continuous-time errors-in-variables models," in *Proc. 16th World Congress Int. Fedeartion Autom. atic Contr.*, Jul. 2005, pp. 3–8.
[22] M. Verhaegen and V. Verdult, *Filtering and System Identification: A Least Squares Approach*. Cambridge, U.K.: Cambridge Univ. Press, 2007.

[23] T. Söderström, L. Ljung, and I. Gustavsson, "A theoretical analysis of recursive identification methods," *Automatica*, vol. 14, no. 3, pp. 231–244, 1978.
[24] J. C. Lagarias, J. A. Reeds, M. H. Wright, and P. E. Wright, "Convergence properties of the nelder-mead simplex method in low dimensions," *SIAM J. Optimiz.*, vol. 9, no. 1, pp. 112–147, 1998.
[25] S. M. LaValle, *Planning Algorithms*. Cambridge, U.K.: Cambridge Univ. Press, 2006.
[26] N. S. Nise, *Control Systems Engineering*, 3rd ed. New York, NY, USA: John Wiley & Sons, 2000.

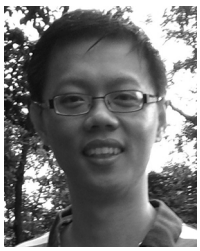

You Hong Eng (S'11–M'14) received the B.Eng. (Hons.) and M.Eng. degrees in mechanical engineering from Nanyang Technological University, Singapore, in 2006 and 2008, respectively. He is currently working toward the Ph.D. degree in industrial and systems engineering at the National University of Singapore.

Since 2008, he has been a Research Associate with the Acoustic Research Laboratory (ARL), Tropical Marine Science Institute. His current research interests are the identification, navigation and control of unmanned underwater vehicles. He is also interested in the development of new types of actuators for underwater applications.

Mr. Eng awards and honors include the Best Student Paper Award at IAENG Conference 2008, the Institution of Engineering and Technology Singapore Branch Book Prize, the Institution Best Student 2004 (NTU) by The Institution of Mechanical Engineers (IMechE), and Meinhardt Book Prize. He is currently the Treasurer of the IEEE Oceanic Engineering Society (OES; Singapore Chapter).

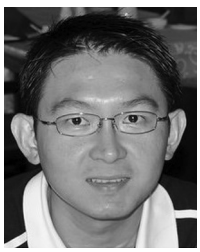

Kwong Meng Teo received the B.Eng. (1st Hons.) degree in electrical and electronics engineering from Institute of Science & Technology , University of Manchester, Manchester , U.K., in 1993, the M.Sc. degree in high performance computation from Singapore-MIT Alliance, Singapore, in 2001, the M.Sc. in electrical engineering from National University of Singapore (NUS), Singapore, in 1997, and the Ph.D. degree in operations research from Massachusetts Institute of Technology's Operations Research Center, Cambridge, MA, USA, in 2007.

He joined NUS in 2009. His research interests lie in optimization and decision making under uncertainties; he enjoys OR applications and systems analysis. Prior to his Ph.D. studies at MIT, he held appointments in the defence industry (C3 systems), application development (supply chain planning), and technical consulting (Operations Research & RFID systems).

Mandar Chitre (S'04–M'05–SM'11) received B.Eng. and M.Eng. degrees in electrical engineering from the National University of Singapore (NUS), Singapore, in 1997 and 2000, respectively, the M.Sc. degree in bioinformatics from the Nanyang Technological University (NTU), Singapore, in 2004, and the Ph.D. degree from NUS, in 2006.

From 1997 to 1998, he worked with the ARL, NUS in Singapore. From 1998 to 2002, he headed the technology division of a regional telecommunications solutions company. In 2003, he rejoined ARL, initially as the Deputy Head (Research) and is now the Head of the laboratory. Dr. Chitre also holds a joint appointment with the Department of Electrical and Computer Engineering at NUS as an Assistant Professor. His current research interests are underwater communications, autonomous underwater vehicles, model-based signal processing and modeling of complex dynamic systems.

Dr. Chitre has served on the technical program committees of the IEEE OCEANS, WUWNet, DTA and OTC conferences and has served as reviewer for numerous international journals. He was the chairman of the student poster committee for IEEE OCEANS06 in Singapore, and the chairman for the IEEE Singapore AUV Challenge 2013. He is currently the IEEE Ocean Engineering Society technology committee cochair of underwater communication, navigation and positioning.

Kien Ming Ng received the B.Sc. (Hons.) degree in mathematics from National University of Singapore, Singapore, in 1994, the M.S. degree in engineering-economic systems and operations research, and the Ph.D. degree in management science and engineering (operations research) from Stanford University, Stanford, CA, USA, in 1999 and 2002, respectively.

From 2002 to 2003, he was a Research Fellow with the Temasek Defence Systems Institute, Singapore. He then joined the Department of Industrial & Systems Engineering, National University of Singapore as an Assistant Professor in 2003 and has been an Associate Professor with the department since 2011. His research interests are in discrete and nonlinear optimization problems arising from the industry and military. Some of the problems that he has worked on include defence logistics and course timetabling problems. His focus is on developing efficient optimization algorithms and techniques to solve such problems, including heuristics for solving scheduling problems, smoothing algorithms for solving nonlinear discrete optimization problems, and metaheuristics for solving routing problems. He is the Managing Editor of the Asia-Pacific Journal of Operational Research.

Dr. Ng has been the President of the Operational Research Society of Singapore since 2011. He is also a member of the Mathematical Optimization Society and the International Council on Systems Engineering.